



Cryo-protective effect of an ice-binding protein derived from Antarctic bacteria

Marco Mangiagalli¹, Maya Bar-Dolev², Pietro Tedesco³, Antonino Natalello¹ , Aleksei Kaleda^{2,4}, Stefania Brocca¹, Donatella de Pascale³, Sandra Pucciarelli⁵, Cristina Miceli⁵, Ido Bravslavsky²  and Marina Lotti¹

¹ Department of Biotechnology and Biosciences, State University of Milano-Bicocca, Italy

² Institute of Biochemistry, Food Science and Nutrition, The Robert H. Smith Faculty of Agriculture, Food and Environment, The Hebrew University of Jerusalem, Rehovot, Israel

³ Institute of Protein Biochemistry, National Research Council, Naples, Italy

⁴ Department of Food Processing, Faculty of Chemical and Materials Technology, Tallinn University of Technology, Estonia

⁵ School of Biosciences and Veterinary Medicine, University of Camerino, Italy

Keywords

cold adaptation; *Euplotes focardii* consortium; ice binding protein; ice recrystallization inhibition; thermal hysteresis

Correspondence

M. Lotti, Department of Biotechnology and Biosciences, State University of Milano Bicocca, Piazza della Scienza 2, 20126 Milano, Italy

Fax: +39 02 6448 3565

Tel: +39 02 6448 3527

E-mail: marina.lotti@unimib.it

(Received 27 July 2016, revised 31 October 2016, accepted 14 November 2016)

doi:10.1111/febs.13965

Cold environments are populated by organisms able to contravene deleterious effects of low temperature by diverse adaptive strategies, including the production of ice binding proteins (IBPs) that inhibit the growth of ice crystals inside and outside cells. We describe the properties of such a protein (*Efc*IBP) identified in the metagenome of an Antarctic biological consortium composed of the ciliate *Euplotes focardii* and psychrophilic non-cultured bacteria. Recombinant *Efc*IBP can resist freezing without any conformational damage and is moderately heat stable, with a midpoint temperature of 66.4 °C. Tested for its effects on ice, *Efc*IBP shows an unusual combination of properties not reported in other bacterial IBPs. First, it is one of the best-performing IBPs described to date in the inhibition of ice recrystallization, with effective concentrations in the nanomolar range. Moreover, *Efc*IBP has thermal hysteresis activity (0.53 °C at 50 μM) and it can stop a crystal from growing when held at a constant temperature within the thermal hysteresis gap. *Efc*IBP protects purified proteins and bacterial cells from freezing damage when exposed to challenging temperatures. *Efc*IBP also possesses a potential N-terminal signal sequence for protein transport and a DUF3494 domain that is common to secreted IBPs. These features lead us to hypothesize that the protein is either anchored at the outer cell surface or concentrated around cells to provide survival advantage to the whole cell consortium.

Introduction

Earth is a cold place where the temperature of over 85% of soil and water environments is close to the freezing point of water. Under these conditions, challenges for life are multifaceted, as temperature affects several key biological processes. In the cold, the

fluidity of cell membranes decreases and protein folding is impaired because hydrophobic interactions weaken. Moreover, the rates of transcription, translation, cell division and chemical reactions slow down. Nevertheless, a rich variety of organisms widely spread

Abbreviations

AFP, antifreeze protein; CFU, colony forming unit; DUF, domain of unknown function; *Efc*IBP, *Euplotes focardii* consortium ice binding protein; FT, freezing and thawing; GFP, green fluorescent protein; IBP, ice binding protein; IBS, ice binding site; IR, ice recrystallization; IRI, ice recrystallization inhibition; LB, Luria-Bertani; PB, phosphate buffer; TB, terrific broth; TH, thermal hysteresis.

across the natural kingdoms thrive in cold habitats [1]. To cope with the constraints mentioned above, the so-called cold-adapted or psychrophilic organisms have evolved different adaptive strategies, for example changes in the composition of cell membranes towards a higher content of unsaturated lipids, and the synthesis of cold-shock proteins and cold-active enzymes [2].

In the extreme condition of permanent subzero temperature, as occurs in permafrost soils and ice seas, or with seasonal fall in temperature another risk threatens even cold-adapted organisms: freezing. The formation of ice crystals both inside and outside cells is a cause of cell damage and death [3]. Fish, insects, plants, algae, diatoms, yeasts and bacteria that colonize very cold habitats, for example Arctic and Antarctic regions, avoid ice injuries by producing ice binding proteins (IBPs), which inhibit the growth of ice crystals [4]. Though all IBPs bind the same ligand – ice – their molecular and functional diversity is astonishing; what surmises recent evolution [4] and makes it difficult to draft a picture of structure–function relationships in this group of proteins. The identification and detailed characterization of novel proteins is expected to add information useful for rationalizing the properties and functions of the IBPs. To this end, this work investigates an IBP from a peculiar biological source, the bacterial community (consortium) that lives in association with a cold-adapted ciliate isolated from cold seawaters at Terranova Bay on the coast of Antarctica.

IBPs decrease the water freezing temperature in a non-colligative manner, thereby creating a hysteresis between the melting and the freezing temperature (thermal hysteresis; TH) [5,6]. TH derives from binding of IBPs to water molecules at the outer layer of ice and inhibiting further ice growth at the position of binding. This local pinning of the surface induces a microcurvature of the rest of the ice surface in between the pinned positions, and makes the association of other water molecules unfavorable from a thermodynamic point of view and *de facto* decreases the water freezing point. IBPs are classified based on their effectiveness in TH. For example, ‘hyperactive’ IBPs from insects and from some bacteria induce TH of 2–13 °C. As the main function of many IBPs is to prevent cell freezing, they are often referred to as ‘antifreeze proteins’. However, IBPs are present also in living beings that have ice crystals within cells or fluids and, therefore, their function is to help cells in tolerating freezing rather than resisting it. In this context, the most remarkable effect of IBPs is the inhibition of ice recrystallization (IR). IR is the growth of large ice crystals at the expenses of smaller ones [7] and is very

harmful for biological matter since it causes dehydration and cellular damage, particularly of cell membranes. Moreover, several microorganisms such as bacteria, fungi, algae and diatoms secrete IBPs to create channels in iced water around cells to allow for the uptake of oxygen and nutrients [8]. Extracellular IBPs contain a conserved region classified in the Pfam database (<http://pfam.xfam.org/>) as ‘domain of unknown function’ (DUF) 3494, and most of them carry a signal peptide for secretion at their amino terminus [8–10].

Crystallographic structures available to date classify IBPs in at least 11 different folds, utilizing different strategies of structural stabilization such as networks of hydrogen bonds and/or disulfide bonds, and/or Ca²⁺ stabilization, whereas the usual hydrophobic core of globular proteins is less relevant [11]. The active site of IBPs is the protein surface devoted to interaction with ice and is called the ice binding site (IBS). Again, different proteins adopt different solutions. Still, common features to most IBSs described to date are that they are quite extended, flat and hydrophobic surfaces and include threonine residues [11]. IBSs are mostly devoid of charged residues and often contain repeated amino acid sequences, consistent with their ability to mimic ice surface [4]. Even more puzzling than structural diversity are the effects of binding of IBPs to ice crystals, since some IBPs are more active in TH and others in IR. Explaining the rationale of such differences is not straightforward [4]. Since it was reported that moderate and hyperactive IBPs bind to different planes of ice crystals [12], the concept was developed that IBP properties depend on their specific spatial interaction with ice [4]. However, what drives IBPs to associate to a specific crystal face is still an open issue.

Here we describe the features of a bacterial ice binding protein, whose coding sequence was found in the metagenome of bacterial symbionts of *Euplotes focardii*, a free-swimming psychrophilic ciliate endemic of the oligotrophic coastal sediments of Terra Nova Bay in Antarctica. Previous studies on this single-cell organism contributed to the understanding of the molecular bases of cold adaptation and suggested a pivotal role for IBPs [13–15]. The sequence studied in this work was identified upon sequencing the *E. focardii* genome. Data analysis showed that out of the 201 918 contigs identified, 11 179 (from 100 to 25 584 bps) did not contain the telomeric repeats typical of *Euplotes* nanochromosomes (CCCCAAA-3′/3′-GGGGTTT-5′) and were attributed to marine bacteria on the basis of a comparison with all bacterial genomes available in the NCBI data bank. Analysis of the 16S RNA sequences [16] revealed that the major

bacterial genera were either Bacteroidetes (16%) or Proteobacteria (78%). Search of IBP sequences within genomic contigs was carried out by Blast analysis, using IBP genes from the diatom *Fragilariopsis cylindrus* as the query. A contig of 3221 bps was found to contain an ORF for a putative IBP of 253 amino acids (GenBank code [AHG59376](#) [15]). In this work, we show that the recombinant protein *E. focardii* consortium IBP (*Efc*IBP) is stable to freezing and thawing, exerts a moderate effect of cryo-protection of pure proteins and whole bacterial cells and displays a remarkable activity in inhibiting ice recrystallization even at very low concentration.

Results

Attempts to produce the recombinant protein *E. focardii* consortium IBP in *Escherichia coli* failed whatever the conditions applied (data not shown). Analysis of sequence AHG59376 by Prosite [17] and SignalP 4.1 [18] suggested that an N-terminal stretch of 23 amino acid residues (MKKIKITMLTATVLFGLLTVVGC) may be a signal for anchorage to the cell surface or for protein transport [15]. Therefore, we designed a sequence devoid of the N-terminal stretch that is referred to in this paper as *Efc*IBP. Production of the recombinant protein was assayed in *E. coli*, at different temperatures and in different growth media as reported in 'Materials and methods'. The highest yield of soluble *Efc*IBP was achieved after 16 h incubation at 25 °C in ZYM-5052 medium [19]. The yield of *Efc*IBP, determined after affinity chromatography purification, was ~ 2 mg from 1 L of culture. Under the same conditions we obtained ~ 8 mg

of green fluorescent protein (GFP) from 1 L of culture (Fig. 1).

Secondary structure and conformational properties of *Efc*IBP

Fourier transform infrared (FTIR) and circular dichroism (CD) spectroscopies were applied to investigate the composition in secondary structure and the conformational stability of *Efc*IBP (Fig. 2). FTIR analysis was performed in the amide I region, where the signal is mainly due to C=O stretching vibrations of the peptide bond, which is particularly sensitive to the polypeptide secondary structures. Figure 2A shows the second derivative spectrum [20] of *Efc*IBP and bands are assigned as described in [21]. The spectrum is dominated by a component at ~ 1634 cm⁻¹, assigned to native β -sheet structures. The component at about 1653 cm⁻¹ occurs in the spectral region of α -helices and random coils, and peaks at ~ 1669 and ~ 1689 cm⁻¹ can be assigned to turn and turn/ β -sheet structures, respectively. The ratio of peak intensity at ~ 1689 and ~ 1634 cm⁻¹ indicates a parallel orientation of the β -sheet structures. Indeed, as suggested by theoretical and experimental works [21,22], in the amide I region the presence of parallel β -sheets is revealed by either a single band at 1640–1623 cm⁻¹ or by this signal together with a very low intensity peak at 1695–1675 cm⁻¹. The high content of β -sheet structures in the *Efc*IBP protein is also highlighted by its CD spectrum displaying a negative band at ~ 219 nm and positive ellipticity at ~ 195 nm (Fig. 2B). Accordingly, the 3D structural model (see later) built using the structure of the IBP from *Flavobacterium frigidis* (33.5% sequence identity) as the template predicts a mainly beta structure.

In order to investigate the robustness of the *Efc*IBP structure towards freezing and towards repeated freezing and thawing (FT) steps, we analysed by FTIR and near-UV CD spectroscopies the structure of the protein stressed by up to 14 FT cycles followed by overnight freezing, as described in 'Materials and methods'.

For the sake of completeness, we show also results obtained with GFP, used as a probe to assess the performance of *Efc*IBP as a cryoprotectant (see later). GFP is similar to *Efc*IBP in size and in the prevalence of beta elements in the secondary structure. Changes in the secondary structure of both proteins revealed by FTIR spectra are hardly detectable (data not shown), whereas effects on the tertiary structures are different and protein dependent (Fig. 3). Indeed, after FT cycles, we observed a small loss of intensity (15% at

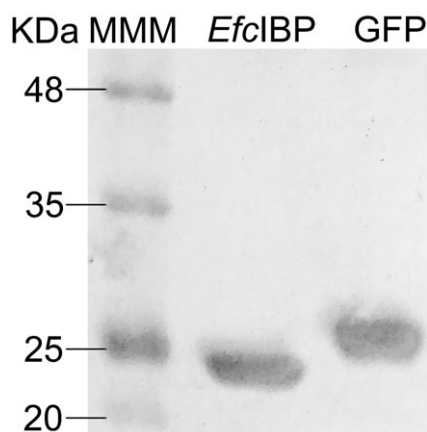


Fig. 1. SDS/PAGE of recombinant proteins purified by affinity chromatography. MMM: molecular mass marker. Each lane contains ~ 5 μ g of purified protein.

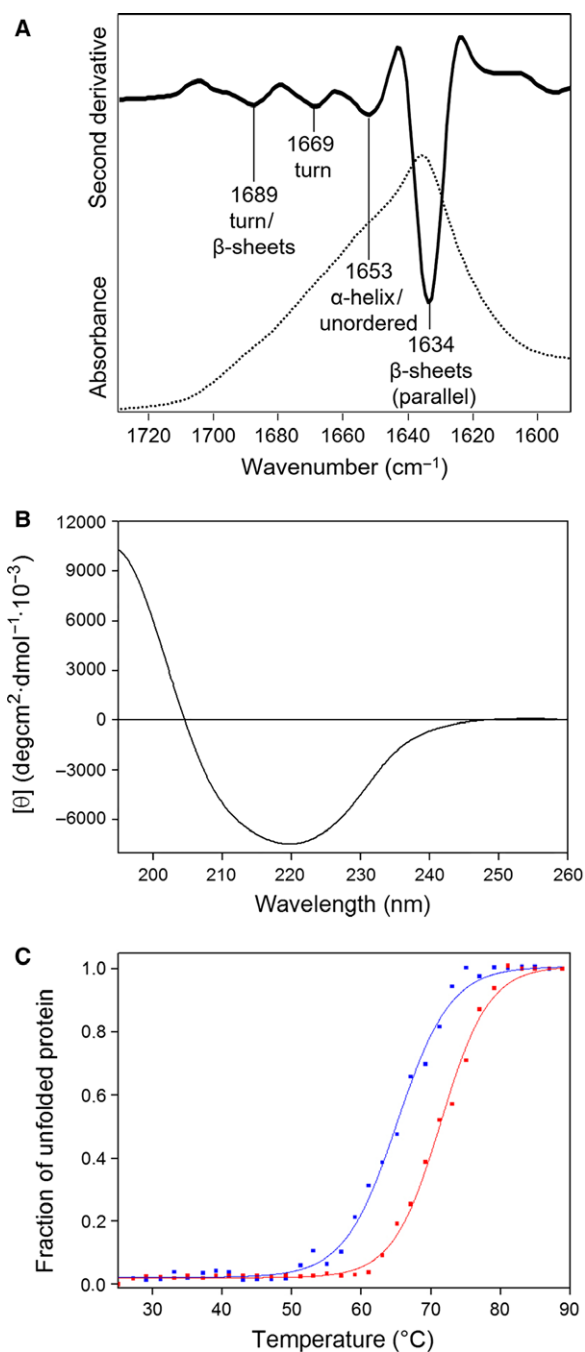


Fig. 2. Secondary structure analysis of *EfcIBP*. (A) FTIR absorption spectrum (dotted line) and second derivative spectrum (continuous line) of *EfcIBP* (40 μM). (B) far-UV CD spectrum of *EfcIBP* (8 μM). (C) Heat stability of *EfcIBP* (blue) and GFP (red) (8 μM). Ellipticity at 215 nm was recorded during heating from 25 to 90 $^{\circ}\text{C}$. Initial CD signal was normalized to 100%.

287 nm) in the near-UV CD spectra of *EfcIBP* (Fig. 3A). Under the same conditions of freeze–thaw cycles, the TH values were not affected. These results

show that structural and functional properties of this IBP are suitable to cope with low temperature and freezing stresses. On the other hand, the spectrum of native GFP revealed a marked flattening of the signal, mainly around 279 nm, where the signal loss is 70% (Fig. 3B).

To gain a more complete view of the protein's temperature sensitivity, we analysed both *EfcIBP* and GFP by CD spectroscopy, monitoring ellipticity changes at 215 nm in samples heated from 25 to 90 $^{\circ}\text{C}$ (Fig. 2C). Above ~ 60 $^{\circ}\text{C}$, the ellipticity signal of *EfcIBP* was rapidly lost with the midpoint at 66.4 ± 2.7 $^{\circ}\text{C}$. The appearance of visible protein precipitates in the cuvette suggested that aggregation occurs. Similar behavior has been reported for *LeIBP* and *FfIBP*, two homologs of *EfcIBP* with midpoint temperature of 61 and 56.4 $^{\circ}\text{C}$, respectively (Table 1) [23]. GFP displayed higher thermal stability with a

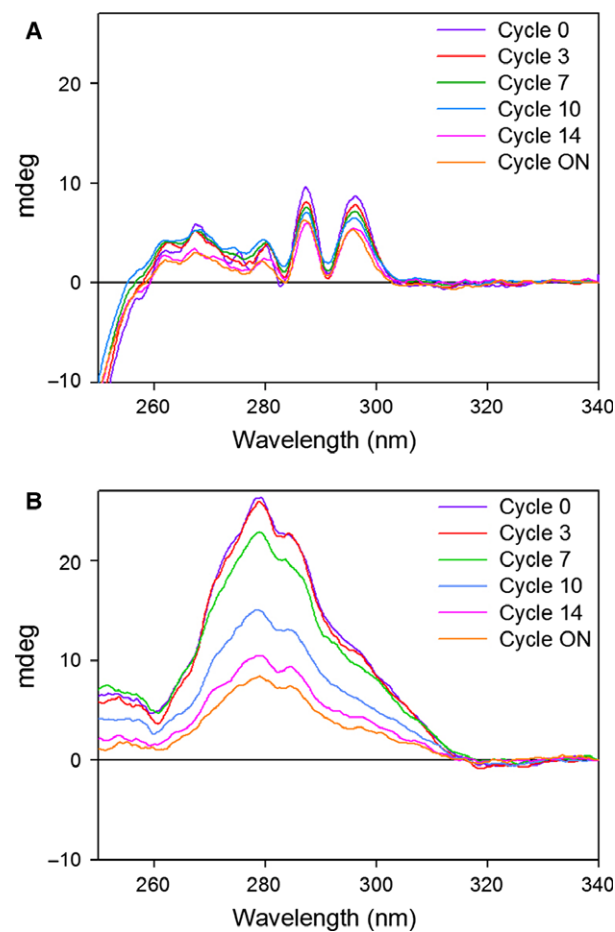


Fig. 3. Robustness of *EfcIBP* (A) and GFP (B) analysed by near-UV CD spectroscopy. Spectra were acquired in phosphate buffer before freezing (cycle 0), upon several cycles of FT and upon further overnight freezing following the 14th FT cycle (cycle ON).

midpoint of signal loss at 71.4 ± 0.8 °C. From these data we surmise that *EfcIBP* not only well withstands repeated freezing and melting, but is also surprisingly thermostable, although less than GFP. Temperature stability of proteins from psychrophilic organisms may sound counterintuitive; however, stability may be a side effect of the rigidity necessary for IBPs when binding to ice crystals. In fact, according to the anchored clathrate waters mechanism, the ice binding sites of IBPs need to be well positioned to allow water molecules to be arranged on top of them in an ice-like structure that mimics ice crystals and allows binding of anchored water to a nearby ice crystal [24].

Ice-binding properties

The thermal hysteresis values of *EfcIBP* are similar to those of moderate fish antifreeze proteins (AFPs) [11] with activity of 0.53 °C at 50 μM concentration, as shown in the TH plot in Fig. 4A. The activity at this concentration did not reach a plateau, indicating that higher concentrations may yield higher TH values. However, higher concentrations are more difficult to measure due to fast melting of superheated crystals. The same TH was obtained with 300 μM (2.1 $\text{mg}\cdot\text{mL}^{-1}$) of AFP type III. In comparison, 40 μM at 8 min incubation time yielded 1.1 °C for the *Tenebrio molitor* AFP, a representative of the hyperactive proteins [25].

The growth and melting patterns observed with *EfcIBP* differ from the bipyramidal patterns obtained with fish AFPs, and have some features similar to the shapes observed with hyperactive insect AFPs [26] and the ryegrass IBP [27] (Fig. 4B). Ice in the presence of *EfcIBP* appears to grow and melt layer by layer in the direction of the basal planes, leading to very thin ice crystals (Video S1). Although the crystals do not grow when held at constant temperatures within the

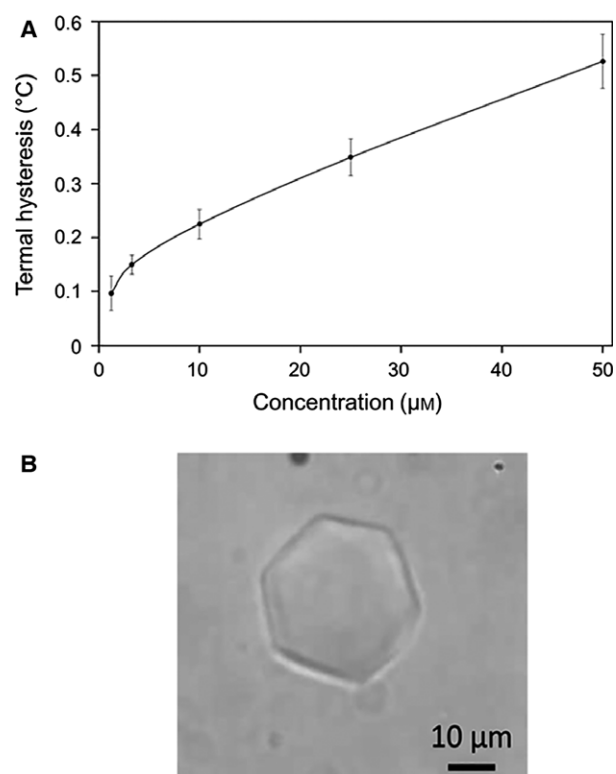


Fig. 4. (A) Thermal hysteresis activity of *EfcIBP*. See text for details. Each data point is the average of at least three measurements. The error bars represent standard deviations ($n = 6$). (B) Ice morphology in the presence of *EfcIBP* (~ 1 μM).

hysteresis gap, stepwise lowering of the temperature leads to step growth of the crystals, until the freezing point is reached and the crystals burst. A similar phenomenon was noted with fish antifreeze glycoproteins, despite differences in crystal morphologies [26]. The step growth was less pronounced at higher concentrations, although it still occurred at 50 μM (1.2 $\text{mg}\cdot\text{mL}^{-1}$). Crystals that grew new ice layers

Table 1. TH activities of *EfcIBP* homologs. Identity with *EfcIBP* was calculated on full-length sequences.

Protein ID	Organism	Identity	TH activity	Reference
<i>EfcIBP</i>	Bacterial consortium of <i>Euplotes focardii</i>	—	0.53 °C at 50 μM	This work
<i>ColAFP</i>	<i>Colwellia</i> sp. strain SLW05	37.3%	3.8 °C at 0.14 mM	[35]
<i>FflBP</i>	<i>Flavobacterium frigoris</i> PS1	33.5%	2.5 °C at 50 μM	[23]
<i>FcAFP</i>	<i>Fragilariopsis cylindrus</i>	30.9%	0.9 °C at 350 μM	[34]
<i>CnAFP</i>	<i>Chaetoceros neogracile</i>	36.3%	0.8 °C at 40 μM	[39]
<i>NaglBP</i>	<i>Navicula glaciei</i>	33.5%	3.2 °C at 1.6 mM	[37]
<i>TisAFP8</i>	<i>Typhula ishikariensis</i>	35.4%	2 °C at 180 μM	[36]
<i>Afp4</i>	<i>Glaciozyma antarctica</i>	31.3%	0.08 °C at 200 μM	[38]
<i>LelBP</i>	<i>Leucosporidium</i> sp. AY30	33.2%	0.35 °C at 370 μM	[33]

within the TH gap did not continue to grow if held at a constant temperature. To check whether the protein accumulates on the ice surface over time, we incubated the crystal in $50\ \mu\text{M}$ *Efc*IBP for 1 or 10 min before temperature lowering. We did not detect any significant difference in TH values, indicating that *Efc*IBP binds quickly (within the first minute) on the crystal surface. Still, after both annealing times, we observed step growth during the temperature decrease.

The IRI activity of *Efc*IBP is shown in Fig. 5. We observed that $0.1\ \mu\text{M}$ of protein was overall sufficient to inhibit IR, but some crystals did grow. At $1\ \mu\text{M}$ *Efc*IBP, IR was completely inhibited. We calculated the IRI efficacy of *Efc*IBP following the analysis derived by Budke *et al.* [28] and compared it with the efficacy of type III AFP from ocean pout (*Zoarces americanus*, QAE (QAE is a particular subgroup of IBPs from ocean pout *Macrozoarces americanus*) isoform named HPLC12) [4]. This fish IBP was chosen as a control since its TH activity is in the same range. The IRI efficacy (C_i) is the inflection point of a curve that describes the dependence of IR rate on protein concentration (Fig. 6). The C_i value represents the concentration of *Efc*IBP below which the IRI is not effective. We found that the C_i of *Efc*IBP is $0.0025 \pm 0.0006\ \mu\text{M}$. For comparison, we measured IRI for ocean pout type III AFP and found a C_i value of $0.05 \pm 0.02\ \mu\text{M}$. The effectivity of *Efc*IBP in IRI is 20-fold higher than type III AFP and it is also very high compared with other IBPs [29,30]. Values of C_i in the nanomolar range were previously reported only for antifreeze glycoproteins [29].

Cryoprotection assays

The biological activity of *Efc*IBP was explored in experiments of cryoprotection of a single pure protein (GFP) and of whole *E. coli* cells. In the first set of experiments, purified GFP was exposed to FT treatment in the presence of $0.6\ \mu\text{M}$ *Efc*IBP or other proteins known to be either active (BSA) or inactive (lysozyme) as cryo-protectors [31]. GFP fluorescence was measured before freezing, after 7 and 14 cycles of FT, and finally after 14 FT cycles and overnight freezing. Under these conditions, we observed a rapid loss of intrinsic fluorescence in GFP (Fig. 7A) likely as a result of denaturation induced by FT treatment and consistent with the results reported in Fig. 3B. The fluorescence decay was milder in the presence of *Efc*IBP and of BSA, but not in the presence of lysozyme, used as a negative control (Fig. 7A).

To evaluate the protection effect of *Efc*IBP on whole cells, we had to perform experiments at less

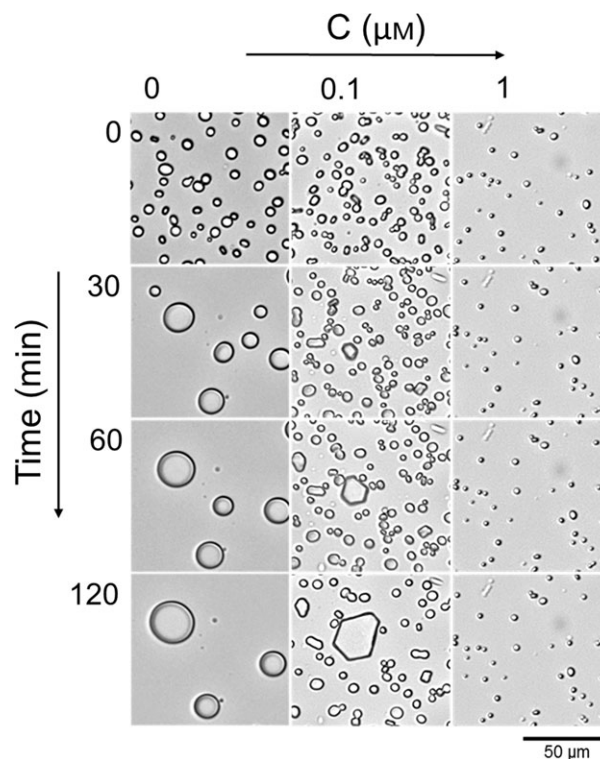


Fig. 5. Ice recrystallization inhibition by *Efc*IBP. A sucrose sandwich assay with and without *Efc*IBP was carried out for 2 h at an annealing temperature of $-7.4\ ^\circ\text{C}$. Snapshots along the experiment are presented. The time lapse is noted to the left. Protein concentration in 45% sucrose solution is noted at the top.

severe temperature, since *E. coli* exposed to FT according to the previous schema was not viable. *E. coli* BL21 (DE3) cells were incubated at a temperature close to the water freezing point in the presence of either 50% (v/v) glycerol or different proteins ($1\ \text{mg}\cdot\text{mL}^{-1}$) as in the previous experiment. Cell viability was assayed every 2 days, by counting colony forming units (CFUs) formed by cells exposed to cold treatment (Fig. 7B). After 12 days, the percentage of viable cells was 6.50% for cells in phosphate buffer (PB) and lysozyme, 9.21% for samples with BSA, 24.6% for samples containing *Efc*IBP and 35% for those with glycerol.

Structure and function in the context of IBP evolution

The maximum likelihood phylogenetic tree (Fig. 8) built with 29 selected sequences from bacteria and eukaryotic microorganism (mostly cold adapted) placed *Efc*IBP within the *Stigmatella aurantica* AFP/IBP lineage. With the exception of *Fimbriimonas*

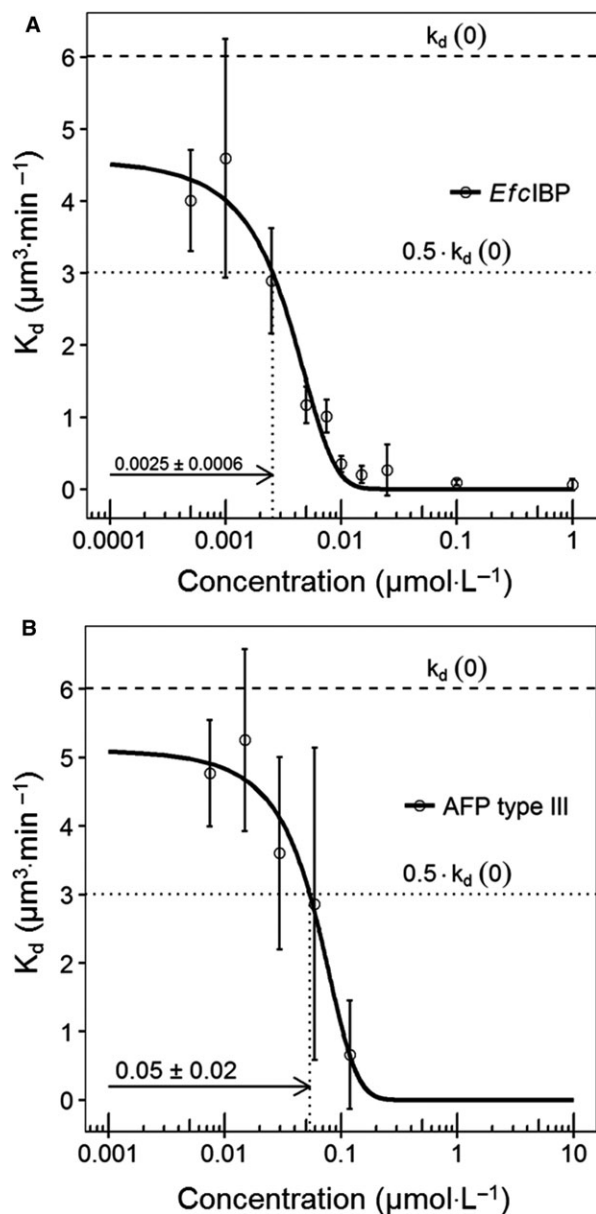


Fig. 6. Quantitative ice recrystallization efficacy of *EfcIBP* and type III AFP. The recrystallization rate constant K_d was measured as a function of protein concentration. Standard deviations are shown ($n = 3$). The inflection point of the curve is the intercept of the dotted lines. The C_i values with 95% confidence intervals are noted at the bottom left. (A) *EfcIBP*. (B) Type III AFP (HPLC12 isoform from ocean pout).

ginsengisoli, the members of the cluster are Antarctic or cryophilic microbes. The same result was obtained when aligned sequences were restricted to 23 IBPs containing a domain of unknown function (DUF) 3494 retrieved from the Pfam server [32] using the *EfcIBP* amino acid sequence as the query (bracketed in Fig. 8).

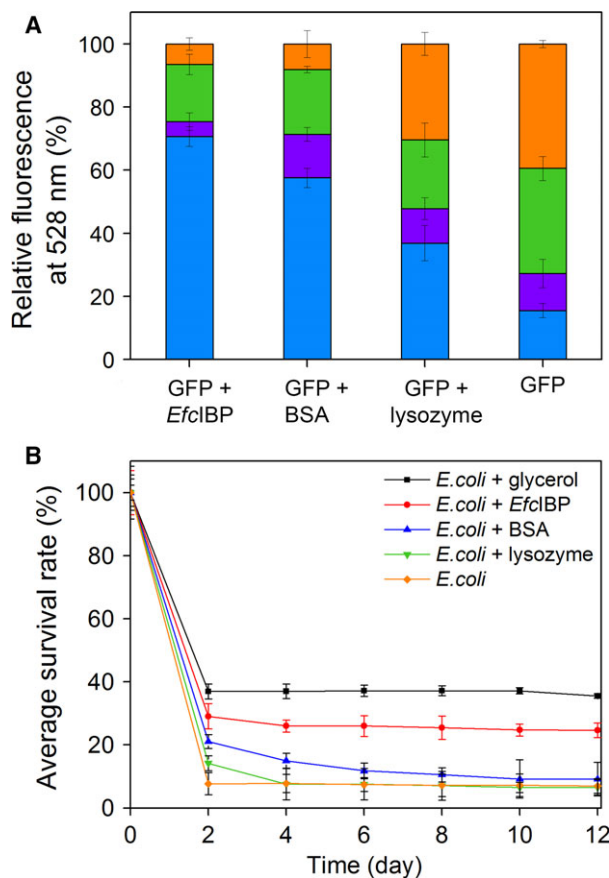


Fig. 7. Cryoprotection assay. (A) Cryoprotection of GFP. GFP fluorescence in the presence of cryoprotectants was acquired before freezing (orange), after 7 (green) and 14 cycles (purple) of FT and after a further overnight freezing following the 14th FT cycle (blue). Initial fluorescence was normalized to 100%. Excitation was at 474 nm and spectra were recorded at 528 nm in PB. Each data point is the average of four measurements. Standard deviations are shown. (B) Cryoprotection of *E. coli* BL21 (DE3) cells. Cells viability in the presence of cryoprotectants was determined in terms of CFUs at different time points in the course of a 12-day incubation at *ca.* 0 °C. For each sample, the number of viable cells before chilling was taken as 100%. Each data point is the average of three measurements. Standard deviations are shown.

To integrate functional and structural analyses, we restricted the cluster to eight IBPs with over 30% sequence identity to *EfcIBP* and whose TH activity had been determined (Table 1) [23,33–39]. The 3D structure of three IBPs included in the comparison (*EfIBP*, *LeIBP* and *ColAFP*) is known and consists of a β -helix with an α -helix alongside the main axes of the protein [23,33,35]. Structural information allowed building the structure-driven multiple alignment shown in Fig. 9. The alignment highlights high

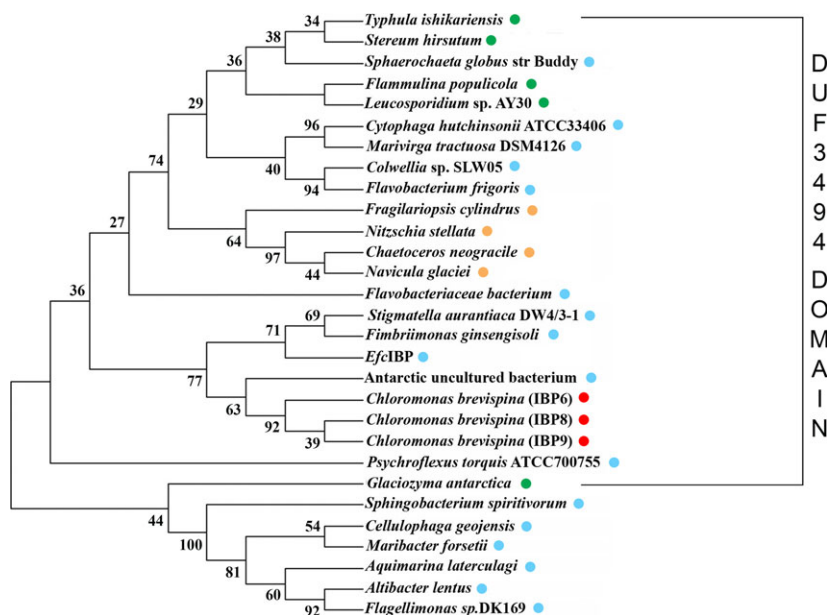


Fig. 8. Phylogenetic tree based on amino acid sequences of ice binding proteins from fungi, bacteria, diatoms and algae (maximum likelihood method on JTT matrix, 1050 bootstraps). Branches reproduced in < 50% of bootstrap replicates are collapsed. The percentage of bootstraps in which the associated taxa clustered together are shown next to the branches. The bullets indicate the sequences obtained from fungi (green), bacteria (blue), diatoms (orange) and algae (red). The sequences were obtained from the NCBI database with the following codes: *Sphaerochaeta globus* (strain Buddy), YP_004248731; *Navicula glaciei*, AAZ76251; *Fragilariopsis cylindrus*, CN212299; *Fragilariopsis curta*, ACT99634; *Chlamydomonas* sp., EU190445; *Typhula ishkarioensis*, BAD02897; *Flammulina populicola*, ACL27144; *Lentinulaedodes edodes*, ACL27145; *Glaciozyma antarctica* ACX31168; *Psychromona ingrahamii*, ZP_01349469; *Colwellia* sp., DQ788793; *Deschampsia antarctica*, ACN38296; *Lolium perenne*, ACN38303, *Marivirga tractuosa* (strain DSM4126), YP_004052221, *Cytophaga hutchinsonii* (strain ATCC33406), YP_676864; *Chaetoceros neogracile*, ACU09498; *Nitzschia stellata*, AEY75833; *Psychroflexus torquis* (strain ATCC700755), YP_006867144; *Stigmatella aurantiaca* (strain DW4/3-1), gi_115375670; an uncultured bacterium (EKD52074.1), *Stereum hirsutum* FP-91666 SS1, XP_007299923.1; Antarctic unidentified bacterium, gi|930810610|gb|ALG05165.1; *Chloromonas brevispina* IBP 6, 8, 9, gi|649907359|gb|AIC65766.1, gi|649907413|gb|AIC65768.1, gi|649907440|gb|AIC65769.1; *Fimbrimonas ginsengisoli* Gsoil 348, gi|663071654|gb|AIE83809.1; *Leucosporidium* sp. AY30 gi|255709878|gb|ACU30806.1.

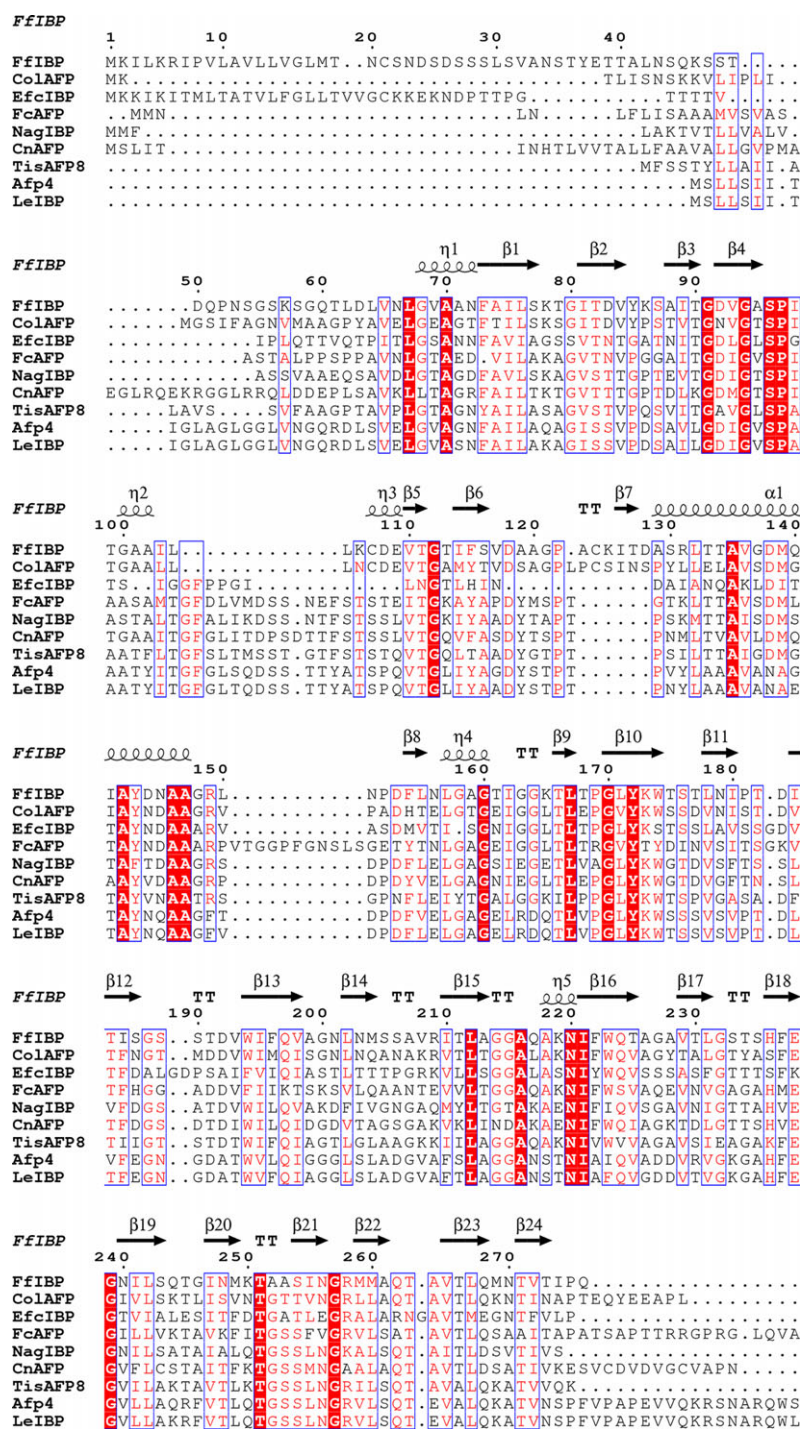
conservation in both primary and secondary structures, as well as in the sequence of IBSs (Fig. 10A), with a mean sequence identity of 26.3%, 23.7% and 23.9% with the IBSs of *FcIBP*, *LeIBP* and *ColAFP*, respectively. A high content of polar residues is observed, in particular threonine and serine. In the structural model, some of these polar amino acids (highlighted in cyan in Fig. 10A) line up on β -sheets, on the same face of the protein, suggesting a putative ice binding face (Fig. 10B). We observed that, in spite of sequence and structure conservation, considered IBPs display different TH activity. We are aware that comparison of TH determined by different authors is not straightforward because of possible discrepancies in concentration and analytical methods. However, with all due caution, data available point to a non-relatedness of general structural organization and TH. Data on IRI, unfortunately, are still too sporadic to be included in the analysis. In

case of *FcAFP*, IRI activity is 1.2 μM and 0.12 μM in low- and high-salinity conditions, respectively [34].

Discussion

As the body of knowledge increases, the heterogeneity of proteins able to bind to ice becomes more and more evident. The widespread occurrence of IBPs within organisms unrelated to each other and the striking variety of sequences, structures and functional strategies is considered proof of recent evolutionary pathways aimed at providing cells and tissues with defences against intracellular and environmental freezing. Polar marine environments are being intensively investigated in the frame of programs for the study and exploitation of biodiversity and provide a rich reservoir of novel organisms.

EfcIBP shows structural and functional properties common to IBPs, but also a combination of TH and



IRI activity not previously described in a bacterial IBP. In particular, we detected a very effective IRI (C_i values of 2.5 nM) showing that *EfcIBP* is among the best performing IBPs described to date. Moreover, *EfcIBP* has TH activity and it can stop a crystal from growing when held at a constant temperature within

the TH gap. Yet the observed stepwise growth of a crystal when the temperature is lowered but not below the hysteresis freezing point indicates that *EfcIBP* is less efficient in preventing ice from growth in these conditions. Altogether these data suggest that freezing point depression is not likely to be the natural role of

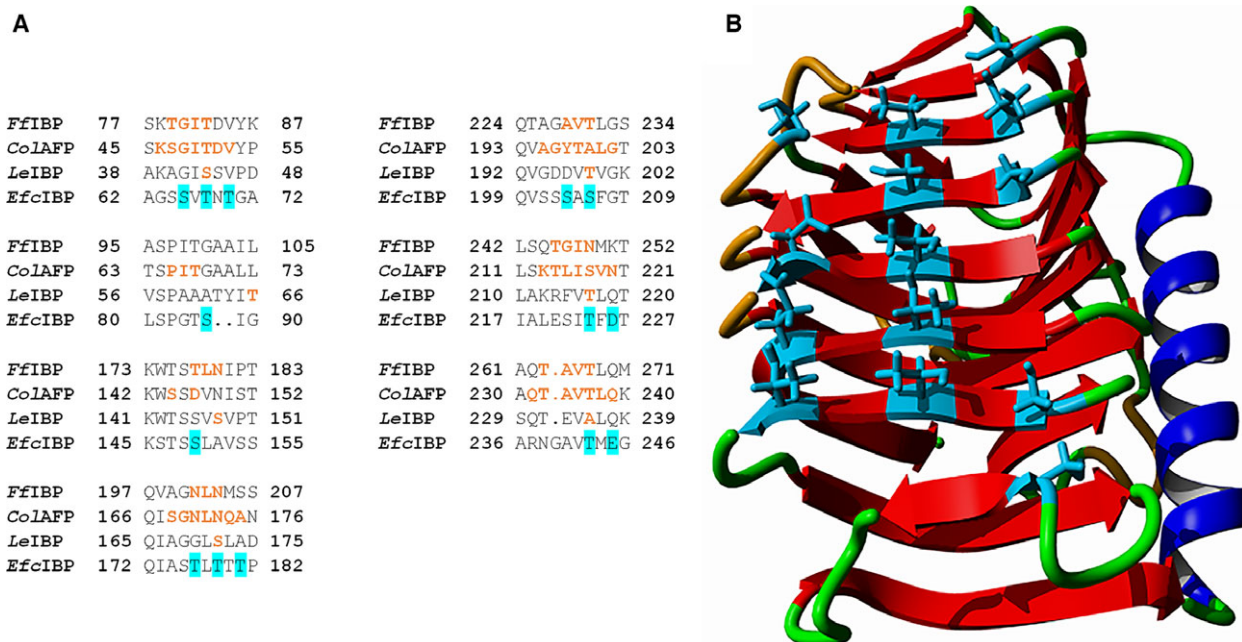


Fig. 10. Ice binding site prediction. (A) Sequence alignment of the IBSPs from *Ff*IBP [23], *Co*IAFP [35], *Le*IBP [33] and *Efc*IBP. The residues involved in ice binding are shown in orange bold. The polar residues located in β -sheet on the same face of *Efc*IBP are highlighted in cyan. The alignment includes the full-length sequence of each protein. (B) Molecular model of *Efc*IBP. The 3D structure was modelled with swiss-MODEL [51] using *Ff*IBP as a template [23]. β -Sheets are indicated in red, α -helices in blue, coils in orange and turns in green; sidechains of polar residues predicted to belong to IBS are in cyan.

this IBP. Rather, *Efc*IBP may serve to depress ice recrystallization or have an effect on preservation of the liquid environment in the vicinity of the consortium. IRI activity was demonstrated in several IBPs secreted by microorganisms that inhabit icy niches, in particular in communities of microorganisms living in sea ice [40]. Such a role would support the importance for *E. focardii* of living together with a bacterial community able to secrete an IBP or at least to export it to the cell surface and is consistent with the cryoprotection effect observed when the IBP is supplemented in sufficient amounts. In the absence of direct evidence about protein transport, the hypothesis of secretion is substantiated by two observations, namely the presence of a putative sequence of transport/anchorage to the cell membrane at the amino terminus and the identification of a DUF3494 domain common to several secreted IBPs [9]. Still to be clarified is the function of this IBP within the cell consortium as it might well be active in the structuring of ice around the ciliate cells but could also play a role when in association with the ciliate cells surface. Such a function has been shown for the Antarctic moss *Bryum argenteum*, which accumulates proteins on its surface [10]. Either anchored at the outer cell surface or concentrated around cells, this protein might provide survival advantages to the entire

consortium and may have contributed to the successful colonization of the Antarctic habitat by the ciliate.

Materials and methods

Strains, media and production assays

E. coli BL21[DE3] (EMD Millipore, Billerica, MA, USA) was used as the host for heterologous expression. Production assays of recombinant *Efc*IBP were carried out in low-salt Luria–Bertani (LB) medium (tryptone 1%, yeast extract 0.5%, sodium chloride 0.5%), terrific broth (TB; tryptone 12%, yeast extract 24%, glycerol 4%, potassium phosphate monobasic 0.17 mM, potassium phosphate dibasic 0.72 mM) or ZYM-5052 medium [19], with addition of 100 mg·L⁻¹ ampicillin. In these analytical experiments, pre-cultures were grown in LB medium to $D_{600} \sim 0.6$ –0.8 and diluted 1 : 25 in different media. Cultures in LB or TB medium were incubated at 30 °C to reach D_{600} 0.6–0.8 before adding 0.2 μ M isopropylthio- β -D-galactoside as inducer. Each induced culture was subdivided in three shaking flasks and incubated at different temperatures (13, 30 and 37 °C). Samples were withdrawn after 2, 4 and 18 h, with additional samples obtained after 48 and 72 h from the 13 °C cultures. Analytical cultures in ZYM-5052 medium were incubated at 13 and 25 °C, for 16–72 h, depending on incubation temperature and samples withdrawn at the end of incubation.

Cloning of the *EfcIBP* coding sequence

The *EfcIBP* gene corresponds to nucleotides 70–762 of the genomic sequence *EfsymbAFP* previously described by [13]. The sequence encoding *EfcIBP* was amplified by PCR using a forward primer (5'-CATATGAAGAAAGAAAAGAACGAT-3') that inserts in 5' the initial ATG along with the restriction site for *NdeI* (underlined) and a reverse primer (5'-CTCGAGCGGCAGAACAAA-3') that inserts in 3' the restriction site for *XhoI* (underlined). Reactions were carried out using MyCycler (Bio-Rad, Hercules, CA, USA) under the following conditions: 1 cycle (95 °C for 5 min), 30 cycles (95 °C 1 min, 54 °C 1 min, and 72 °C 1 min), and a final cycle of 72 °C for 7 min. PCR products were cloned in frame with a sequence coding for C-terminal 6xHis-Tag into the pET-21a expression vector previously cleaved with *NdeI* and *XhoI* to obtain pET-21a[*EfcIBP*]. The sequence of cloned DNA was verified by bidirectional DNA sequencing.

GFP was produced from pET-19b [GFP] [41]. Type III AFP is a recombinant version of HPLC12, a type III isoform that belongs to the QAE subgroup of IBPs from ocean pout *M. americanus*. The protein was produced in *E. coli* and purified as described elsewhere [42].

Production and purification of recombinant proteins

Production of recombinant *EfcIBP* and GFP was in ZYM-5052 [19] with addition of 100 mg·L⁻¹ ampicillin. Pre-cultures were grown in low-salt LB medium up to $D_{600} \sim 0.6$ –0.8, diluted 1 : 25 in ZYM-5052 and incubated overnight at 25 °C.

Proteins were purified by affinity chromatography using resin of nickel–nitrilotriacetic acid agarose. Elution fractions containing the highest protein concentrations were pooled and buffer was exchanged for 10 mM ammonium acetate pH 7.0 by two consecutive gel filtrations on PD-10 columns (GE Healthcare, Little Chalfont, UK) according to the manufacturer's instructions. Samples were lyophilized in a freeze-dryer (Heto FD1.0, Gemini BV, Apeldoorn, the Netherlands) and stored at -20 °C or re-suspended in PB (25 mM sodium phosphate pH 7.0).

Protein concentration was determined by the Bradford protein assay (Bio-Rad), using bovine serum albumin as the standard. SDS/PAGE was on 14% acrylamide gels [43] stained with Coomassie dye (Bio-Rad) after electrophoresis. Broad-range, pre-stained molecular-mass markers (Gene-Spin, Milan, Italy) were used as standards.

Analysis of protein conformation and stability

CD spectroscopy

CD spectra of proteins dissolved in PB (8 μM for far-UV measurements and 40 μM for near-UV measurements) were

recorded with a J-815 spectropolarimeter (Jasco Corp., Easton, MD, USA), using either 0.1 cm (for far-UV) or 1 cm path length quartz cuvettes (for near-UV). Experiments were in duplicate.

Spectra in the far-UV were measured in the range 195–260 nm, while near-UV measurements were at 240–340 nm, with 0.1 nm data pitch and 20 nm·min⁻¹ scanning speed. All spectra were corrected for buffer contribution, averaged from two independent acquisitions, and smoothed by using a third-order least square polynomial fit.

Thermal denaturation spectra were obtained measuring the CD signal at 215 nm fixed wavelength when progressively heating the sample from 25 to 90 °C. Measurements were performed with a data pitch of 0.2 °C and a temperature slope of 5 °C·min⁻¹.

Molar mean ellipticity values per residue $[\theta]$ were calculated as:

$$[\theta] = \frac{3300 \cdot m \cdot \Delta A}{c \cdot n \cdot l}$$

where ΔA is the difference in the absorption between circularly polarized right and left light of the protein corrected for blank, m is the protein molecular mass in daltons, l is the path length (0.1 cm), c is the protein concentration (mg·mL⁻¹) and n is the number of residues [41].

FTIR spectroscopy

FTIR spectra in attenuated total reflection (ATR) were collected by using the Quest device (Specac, UK) equipped with a single reflection diamond element. Aliquots of 2 μL of protein solution (40 μM in PB) were deposited on the ATR plate and dried at room temperature in order to obtain a protein film. ATR/FTIR spectra were then measured using a Varian 670-IR spectrometer (Varian Australia Pty Ltd, Mulgrave, Victoria, Australia) under the following conditions: 2 cm⁻¹ spectral resolution, 25 kHz scan speed, 512 scan co-additions, triangular apodization and nitrogen-cooled mercury cadmium telluride detector. Absorption spectra were corrected for buffer contribution, and normalized to the amide I band intensity. Analyses of spectra were performed with the software Resolutions-Pro (Varian Australia).

Assessment of stability to freezing and thawing

IBP and GFP samples (40 μM) were subjected to up to 14 cycles of freezing (-20 °C for 20 min) and thawing (25 °C for 10 min) or to 14 cycles of FT followed by overnight freezing (-20 °C for 16 h). Effects on protein structure were assessed by near-UV CD and FTIR spectroscopies.

Ice binding assays

Thermal hysteresis and ice crystal morphology

We observed ice morphologies and determined TH using a LabVIEW (National Instruments Corp., Austin, TX, USA)-operated custom-designed nanoliter osmometer as described [44,45]. Lyophilized proteins were recovered in double distilled water to 50 μM solution and diluted in 20 mM ammonium bicarbonate (pH 8.5). Rehydrated proteins exhibit the same secondary structure of freshly prepared, soluble samples, as revealed by FTIR spectra (data not shown). Samples of ~ 10 nL immersed in oil were cooled until freezing (~ -30 °C) and then warmed until a single ice crystal of < 20 μm diameter remained. The melting temperature of the crystal was measured and then the crystal was incubated for 1 or 10 min at a few hundredths of a degree below the melting point. After incubation, the temperature was reduced by 0.01 °C every 4 or 10 s and the crystal image was recorded. The temperature at which fast growth commenced was determined as the freezing point. The difference between the melting point and the hysteresis freezing points is the TH value.

Ice recrystallization inhibition

Ice recrystallization inhibition (IRI) was conducted using a sucrose-sandwich assay [46] with some modifications [28]. The final solutions contained 45% sucrose, 50 mM NaCl, 10 mM Tris (pH 8.0) and up to 1 μM of protein. Samples of 1 μL were placed on a sapphire sample holder and covered with a 13-mm diameter circular glass coverslip. The sapphire was used to reduce temperature gradients. The sample was sealed with type-B immersion oil (Sigma-Aldrich, St. Louis, MO, USA) to avoid evaporation and mounted on the stage of a Motorized Cryobiology System (model MDBCS196, Linkam Scientific, Tadworth, UK). A copper plate with a 2.5-mm diameter slit was placed on top of the sample to further reduce temperature gradients. Immersion oil was used between the sample, the stage and the slit to improve thermal contact. The Linkam stage was placed on a light microscope (BX41, Olympus America Inc., Melville, NY, USA) and operated using a Labview interface. The system was cooled from room temperature to -50 °C at a rate of 130 °C $\cdot\text{min}^{-1}$ and sustained at -50 °C for 1 min. The temperature was then elevated to -20 °C at a warming rate of 130 °C $\cdot\text{min}^{-1}$ and then warming continued to -10 °C at a rate of 10 °C $\cdot\text{min}^{-1}$. The final stage of heating up to the annealing temperature of -7.4 °C was conducted at a slow rate of 1 °C $\cdot\text{min}^{-1}$ to avoid overheating. The sample was maintained at this temperature for 60 min. During this period, recrystallization was recorded using an EXi Aqua bio-Imaging camera (QImaging, Surrey, Canada) every 1 min. The experiment was carried out with different concentrations of protein and repeated at least three times for each concentration.

The IRI was calculated following the mathematical description derived by Budke *et al.* [28]. The images were processed using Fiji (R Foundation for Statistical Computing, Vienna, Austria) to calculate the number of crystals, the mean radius of the crystals and the total crystal volume. The cube of the mean crystal radius was calculated for all images in each data set and plotted against time. The slope of the curve obtained from time points 30–60 min was taken as the recrystallization rate constant. The ice volume fraction (Q) was also calculated for all images in each data set and only experiments with $< 1\%$ variation in Q were considered. In all experiments the ice volume fraction was up to 9% (in high volume fraction the theory for IRI calculation is not legitimate). The recrystallization rates (K_d) were plotted against protein concentration, with at least three replicates for each concentration. This data set was fitted to a sigmoidal curve using R (R Foundation for Statistical Computing, Vienna, Austria). The inflection point of the curve, termed the C_i value, represents the effective protein concentration below which recrystallization is not efficiently inhibited [28]. A profile likelihood confidence interval ($\alpha = 0.05$) for the C_i point was calculated using the 'nlstools' R package. The rate constant in the absence of protein ($K_d(Q)$ at $[C] = 0$) was determined by measuring the recrystallization rate of buffer without protein. This experiment was repeated eight times and the averaged $K_d(Q)$ value was used for curve fitting. To accommodate the possible effects of different Q , we extrapolated all K_d values for zero volume fraction $Q = 0$ as described [28] and plotted the new K_{10} values against protein concentration (data not shown). The difference between the original C_i value and the corrected C_i value was very small.

Cryoprotection assays

Cryoprotection of GFP

Fluorescence spectroscopy experiments were carried out to detect the effects of FT on GFP fluorescence in either the presence or the absence of the *EfcIBP*. All protein samples were dissolved or prepared in PB. Samples of GFP (0.6 μM) were mixed with equimolar concentrations of *EfcIBP*, BSA (Sigma-Aldrich), or lysozyme (Sigma-Aldrich) or with PB alone, in a final volume of 500 μL in PB. Samples were divided into four 100 μL aliquots and deposited in a 96-multiwell plate to replicate each measurement. Plates were then frozen and thawed according to the scheme previously described above in 'Assessment of stability to freezing and thawing'. Emission spectra were recorded before freezing, after 7 and 14 FT cycles and finally after overnight freezing. Fluorescence emitted from GFP was measured by a Cary Eclipse (Varian Inc., Palo Alto, CA, USA) spectrofluorimeter using 96-multiwell plates. GFP fluorescence was recorded at room temperature

with excitation at 474 nm and emission at 528 nm. The experiment was repeated three times.

Cold-tolerance assays were carried out on *E. coli* BL21 (DE3) cells exposed to low temperature in the presence or in the absence of *Efc*IBP. Cells carrying empty plasmid pET21 (to confer ampicillin resistance) were grown in ZYM-5052 medium and incubated overnight at 25 °C until they reached a D_{600} of ~ 3 . Aliquots of 1 mL of fresh culture were mixed with equal volumes of 1 mg·mL⁻¹ PB solutions of *Efc*IBP, BSA (Sigma-Aldrich), lysozyme (Sigma-Aldrich), or glycerol (50%) (Euroclone, Pero, Italy), or with PB alone as a control. Cell aliquots in 1.5-mL plastic tubes were kept submerged in ice for several days at a temperature of -0.5 °C. After 0, 2, 4, 6, 8, 10 and 12 days, samples were diluted in LB medium with addition of 100 mg·L⁻¹ ampicillin, and inoculated on LB-agar plates to count CFUs after 16 h incubation at 37 °C. Plates were inoculated in three replicates for each point.

Sequence analysis and modelling of 3D structure

The evolutionary history was inferred by using the maximum likelihood method based on the JTT matrix-based model [47]. The bootstrap consensus tree was inferred from 1050 replicates and assumed to describe the evolutionary history of the analyzed taxa [48]. An initial tree for the heuristic search was obtained by applying the neighbor-joining method to a matrix of pairwise distances estimated using a JTT model. The analysis involved 29 amino acid sequences. There was a total of 792 positions in the final dataset. Evolutionary analyses were conducted with MEGA5 [49]. Multiple alignments were performed by ESPRIT [50]. The 3D structure of *Efc*IBP was modelled on the structure of *Fj*IBP (PDB: 4NU2 [23]) using SWISS-MODEL [51]. *Efc*IBP displays a sequence identity of 33.5% compared with the *Fj*IBP. The resulting model was visualized using YASARA (www.yasara.org) and POVray (www.povray.org).

Acknowledgements

This work was supported by a grant of the Progetto Nazionale di Ricerche in Antartide PEA 2014-2016 entitled ‘Genome scanning and characterization of novel antifreeze proteins for industrial application’ coordinated by DdP and by a grant of ERC to IB. AK acknowledges support by the Estonian national scholarship program Kristjan Jaak. We thank Dr Victor Yashunsky (The Hebrew University of Jerusalem, Israel), and Dr Lior Segev (Weizmann Institute of Science, Israel) for LabVIEW programming and Lotem Haleva for her contribution to TH thermal stability analysis.

Author contributions

MM and SB carried out production and purification of the recombinant proteins and assessed stability and cryoprotection activity; AN performed analyses by infrared spectroscopy; MB-D, AK and IB characterized the TH and IRI activity and studied ice crystals morphology; PT and DdeP designed and produced the coding sequence; SP and CM performed evolutionary analysis; DdeP and ML conceived and supervised the project; ML wrote the paper. All Authors have read and approved the content of the manuscript.

References

- De Maayer P, Anderson D, Cary C & Cowan DA (2014) Some like it cold: understanding the survival strategies of psychrophiles. *EMBO Rep* **15**, e201338170.
- D’Amico S, Collins T, Marx JC, Feller G & Gerday C (2006) Psychrophilic microorganisms: challenges for life. *EMBO Rep* **7**, 385–389.
- Bouvet V & Ben RN (2003) Antifreeze glycoproteins – Structure, conformation, and biological applications. *Cell Biochem Biophys* **39**, 133–144.
- Bar Dolev M, Braslavsky I & Davies PL (2016) Ice-binding proteins and their function. *Annu Rev Biochem* **85**, 515–542.
- Raymond JA & DeVries AL (1977) Adsorption inhibition as a mechanism of freezing resistance in polar fishes. *Proc Natl Acad Sci USA* **74**, 2589–2593.
- DeVries AL, Komatsu SK & Feeney RE (1970) Chemical and physical properties of freezing point-depressing glycoproteins from Antarctic fishes. *J Biol Chem* **245**, 2901–2908.
- Knight CA, DeVries AL & Oolman LD (1984) Fish antifreeze protein and the freezing and recrystallization of ice. *Nature* **308**, 295–296.
- Davies PL (2016) Antarctic moss is home to many epiphytic bacteria that secrete antifreeze proteins. *Environ Microbiol Rep* **8**, 1–2.
- Raymond JA (2014) The ice-binding proteins of a snow alga, *Chloromonas brevispina*: probable acquisition by horizontal gene transfer. *Extremophiles* **18**, 987–994.
- Raymond JA (2015) Dependence on epiphytic bacteria for freezing protection in an Antarctic moss, *Bryum argenteum*. *Environ Microbiol Rep* **8**, 14–19.
- Davies PL (2014) Ice-binding proteins: a remarkable diversity of structures for stopping and starting ice growth. *Trends Biochem Sci* **39**, 548–555.
- Drori R, Celik Y, Davies PL & Braslavsky I (2014) Ice-binding proteins that accumulate on different ice crystal planes produce distinct thermal hysteresis dynamics. *J R Soc Interface* **11**, 20140526.

- 13 Pucciarelli S, La Terza A, Ballarini P, Barchetta S, Yu T, Marziale F, Passini V, Methe B, Detrich HW III & Miceli C (2009) Molecular cold-adaptation of protein function and gene regulation: the case for comparative genomic analyses in marine ciliated protozoa. *Mar Genomics* **2**, 57–66.
- 14 Yang G, De Santi C, de Pascale D, Pucciarelli S, Pucciarelli S & Miceli C (2013) Characterization of the first eukaryotic cold-adapted patatin-like phospholipase from the psychrophilic Euplotes focardii: identification of putative determinants of thermal-adaptation by comparison with the homologous protein from the mesophilic Euplotes crassus. *Biochimie* **95**, 1795–1806.
- 15 Pucciarelli S, Chiappori F, Devaraj RR, Yang G, Yu T, Ballarini P & Miceli C (2014) Identification and analysis of two sequences encoding ice-binding proteins obtained from a putative bacterial symbiont of the psychrophilic Antarctic ciliate Euplotes focardii. *Antarct Sci* **26**, 491–501.
- 16 Pucciarelli S, Devaraj RR, Mancini A, Ballarini P, Castelli M, Schrallhammer M, Petroni G & Miceli C (2015) Microbial Consortium Associated with the Antarctic Marine Ciliate Euplotes focardii: an investigation from genomic sequences. *Microb Ecol* **70**, 484–497.
- 17 Sigrist CJA, de Castro E, Cerutti L, Cuche BA, Hulo N, Bridge A, Bougueleret L & Xenarios I (2013) New and continuing developments at PROSITE. *Nucleic Acids Res* **41**, E344–E347.
- 18 Petersen TN, Brunak S, von Heijne G & Nielsen H (2011) SignalP 4.0: discriminating signal peptides from transmembrane regions. *Nat Methods* **8**, 785–786.
- 19 Studier FW (2005) Protein production by auto-induction in high-density shaking cultures. *Protein Expr Purif* **41**, 207–234.
- 20 Byler DM & Susi H (1986) Examination of the secondary structure of proteins by deconvolved FTIR spectra. *Biopolymers* **25**, 469–487.
- 21 Barth A (2007) Infrared spectroscopy of proteins. *Biochim Biophys Acta* **1767**, 1073–1101.
- 22 Cerf E, Sarroukh R, Tamamizu-Kato S, Breydo L, Derclaye S, Dufrene Y, Narayanaswami V, Goormaghtigh E, Ruyschaert J & Raussens V (2009) Antiparallel beta-sheet: a signature structure of the oligomeric amyloid beta-peptide. *Biochem J* **421**, 415–423.
- 23 Do H, Kim SJ, Kim HJ & Lee JH (2014) Structure-based characterization and antifreeze properties of a hyperactive ice-binding protein from the Antarctic bacterium *Flavobacterium frigidum* PS1. *Acta Crystallogr D* **70**, 1061–1073.
- 24 Garnham CP, Campbell RL & Davies PL (2011) Anchored clathrate waters bind antifreeze proteins to ice. *Proc Natl Acad Sci USA* **108**, 7363–7367.
- 25 Graham LA, Liou YC, Walker VK & Davies PL (1997) Hyperactive antifreeze protein from beetles. *Nature* **388**, 727–728.
- 26 Bar-Dolev M, Celik Y, Wettlaufer JS, Davies PL & Braslavsky I (2012) New insights into ice growth and melting modifications by antifreeze proteins. *J R Soc Interface* **9**, 3249–3259.
- 27 Middleton AJ, Marshall CB, Faucher F, Bar-Dolev M, Braslavsky I, Campbell RL, Walker VK & Davies PL (2012) Antifreeze protein from freeze-tolerant grass has a beta-roll fold with an irregularly structured ice-binding site. *J Mol Biol* **416**, 713–724.
- 28 Budke C, Heggemann C, Koch M, Sewald N & Koop T (2009) Ice recrystallization kinetics in the presence of synthetic antifreeze glycoprotein analogues using the framework of LSW theory. *J Phys Chem B* **113**, 2865–2873.
- 29 Budke C, Dreyer A, Jaeger J, Gimpel K, Berkemeier T, Bonin AS, Nagel L, Plattner C, DeVries AL & Sewald N (2014) Quantitative efficacy classification of ice recrystallization inhibition agents. *Cryst Growth Des* **14**, 4285–4294.
- 30 Olijve LLC, Meister K, DeVries AL, Duman JG, Guo S, Bakker HJ & Voets IK (2016) Blocking rapid ice crystal growth through nonbasal plane adsorption of antifreeze proteins. *Proc Natl Acad Sci USA* **113**, 3740–3745.
- 31 Hughes S & Graether SP (2011) Cryoprotective mechanism of a small intrinsically disordered dehydrin protein. *Protein Sci* **20**, 42–50.
- 32 Finn RD, Coghill P, Eberhardt RY, Eddy SR, Mistry J, Mitchell AL, Potter SC, Punta M, Qureshi M & Sangrador-Vegas A (2016) The Pfam protein families database: towards a more sustainable future. *Nucleic Acids Res* **44**, D279–D285.
- 33 Lee JH, Park AK, Do H, Park KS, Moh SH, Chi YM & Kim HJ (2012) Structural basis for antifreeze activity of ice-binding protein from arctic yeast. *J Biol Chem* **287**, 11460–11468.
- 34 Bayer-Giraldi M, Weikusat I, Besir H & Dieckmann G (2011) Characterization of an antifreeze protein from the polar diatom *Fragilariopsis cylindrus* and its relevance in sea ice. *Cryobiology* **63**, 210–219.
- 35 Hanada Y, Nishimiya Y, Miura A, Tsuda S & Kondo H (2014) Hyperactive antifreeze protein from an Antarctic sea ice bacterium *Colwellia* sp has a compound ice-binding site without repetitive sequences. *FEBS J* **281**, 3576–3590.
- 36 Xiao N, Suzuki K, Nishimiya Y, Kondo H, Miura A, Tsuda S & Hoshino T (2010) Comparison of functional properties of two fungal antifreeze proteins from *Antarctomyces psychrotrophicus* and *Typhula ishikariensis*. *FEBS J* **277**, 394–403.
- 37 Xiao N, Hanada Y, Seki H, Kondo H, Tsuda S & Hoshino T (2014) Annealing condition influences

- thermal hysteresis of fungal type ice-binding proteins. *Cryobiology* **68**, 159–161.
- 38 Hashim NHF, Sulaiman S, Bakar FDA, Illias RM, Kawahara H, Najimudin N, Mahadi NM & Murad AMA (2014) Molecular cloning, expression and characterisation of Afp4, an antifreeze protein from *Glaciozyma antarctica*. *Polar Biol* **37**, 1495–1505.
- 39 Gwak IG, sic Jung W, Kim HJ, Kang S-H & Jin E (2010) Antifreeze protein in Antarctic marine diatom, *Chaetoceros Neogracile*. *Mar Biotechnol* **12**, 630–639.
- 40 Uhlig C, Kilpert F, Frickenhaus S, Kegel JU, Krell A, Mock T, Valentin K & Beszteri B (2015) In situ expression of eukaryotic ice-binding proteins in microbial communities of Arctic and Antarctic sea ice. *ISME J* **9**, 2537–2540.
- 41 Sambti I, Gatti-Lafranconi P, Longhi S & Lotti M (2010) How disorder influences order and vice versa – mutual effects in fusion proteins containing an intrinsically disordered and a globular protein. *FEBS J* **277**, 4438–4451.
- 42 DeLuca CI, Comley R & Davies PL (1998) Antifreeze proteins bind independently to ice. *Biophys J* **74**, 1502–1508.
- 43 Laemmli UK (1970) Cleavage of structural proteins during the assembly of the head of bacteriophage T4. *Nature* **227**, 680–685.
- 44 Braslavsky I & Drori R (2013) LabVIEW-operated novel nanoliter osmometer for ice binding protein investigations. *J Vis Exp* **72**, e4189.
- 45 Pertaya N, Celik Y, DiPrinzio CL, Wettlaufer JS, Davies PL & Braslavsky I (2007) Growth-melt asymmetry in ice crystals under the influence of spruce budworm antifreeze protein. *J Phys Condens Matter* **19**, 412101.
- 46 Regand A & Goff HD (2006) Ice recrystallization inhibition in ice cream as affected by ice structuring proteins from winter wheat grass. *J Dairy Sci* **89**, 49–57.
- 47 Jones DT, Taylor WR & Thornton JM (1992) The rapid generation of mutation data matrices from protein sequences. *Comput Appl Biosci* **8**, 275–282.
- 48 Felsenstein J (1985) Confidence limits on phylogenies: an approach using the bootstrap. *Evolution* **39**, 783–791.
- 49 Tamura K, Peterson D, Peterson N, Stecher G, Nei M & Kumar S (2011) MEGA5: molecular evolutionary genetics analysis using maximum likelihood, evolutionary distance, and maximum parsimony methods. *Mol Biol Evol* **28**, 2731–2739.
- 50 Robert X & Gouet P (2014) Deciphering key features in protein structures with the new ENDscript server. *Nucleic Acids Res* **42**, W320–W324.
- 51 Biasini M, Bienert S, Waterhouse A, Arnold K, Studer G, Schmidt T, Kiefer F, Cassarino TG, Bertoni M & Bordoli L (2014) SWISS-MODEL: modelling protein tertiary and quaternary structure using evolutionary information. *Nucleic Acids Res* **42**, W252–W258.

Supporting information

Additional Supporting Information may be found online in the supporting information tab for this article: **Video S1**. Ice crystal growth. A single ice crystal grown in a solution containing 3.3 μM *Efc*IBP (melting temperature = -0.02).